Inorganic Chemistry
Cite This: Inorg. Chem. XXXX, XXX, XXX−XXX
Article
pubs.acs.org/IC

Quantifying Ligand Exchange on InP Using an Atomically Precise Cluster Platform

Andrew Ritchhart and Brandi M. Cossairt*

Department of Chemistry, University of Washington, Seattle, Washington 98195-1700, United States

Supporting Information

ABSTRACT: The surface chemistry of a colloidal nanoparticle is intrinsic to both its structure and function. It is therefore necessary to characterize the surfaces of colloidal materials to rationally underpin any synthetic, catalytic, or transformative mechanisms they enable. Here we characterize the surface properties of colloidal InP clusters and quantum dots by examining the binding of traditional stabilizing ligands including carboxylates, phosphonates, and thiolates. By using the $In_{37}P_{20}X_{51}$ (X = carboxylate) cluster species as an ideally monodisperse and well-defined starting scaffold, we quantify surface-exchange equilibria. Using quantitative ^{1}H and ^{31}P NMR spectroscopy, we show that 1:1 metathesis-type binding models are insufficient to fully describe the surface dynamics. In particular, for the case of the highly reversible carboxylate ligand exchange, a more detailed isotherm approach using a two-site, competitive model is necessary. This model is used to deconvolute L- and X-type binding modalities. We additionally quantify the reversible and irreversible ligand-exchange reactions observed in the thiolate and phosphonate systems.

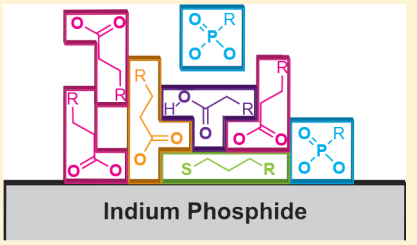

INTRODUCTION

Our understanding of the chemistry of colloidal semiconductor nanoparticles has advanced to enable progress in applying these materials in a wide range of applications including catalysis,[1,2] photovoltaics,[3,4] displays,[5] and imaging.[6,7] Recent efforts have focused on developing nontoxic materials, such as InP, for large-scale, highly distributed applications.[8,9] Research into II−IV and III−V nanomaterials has been tailored to the applications at hand by manipulating the quantum confinement effect as a function of the size,[10,11] shape,[12,13] and composition.[14] Underpinning this research, and fundamental to colloidal nanoparticle function and synthesis, is the nature of the nanoparticle surface. The surface and ligand layer represent a highly complex component of the nanoparticle composition that has influence on the structural, electronic, and reactivity properties of the nanomaterial.[15,16] Accurately quantifying the binding properties of ligands is critical for the design of size-tunable and anisotropic nanoparticle syntheses,[17,18] as well as for postsynthetic modifications such as shelling, passivation, or cation exchange.[19−21] A detailed, analytical understanding of the surface structure and ligand coordination properties of a colloidal system must underscore any rational design of the nanoscale properties in those systems.

Postsynthetic ligand modification specifically has enabled a host of targeted applications. Exchanging ligands of differing hydrophobicity has long been known to facilitate changes in the nanoparticle solubility, a critical parameter to control applications in biosensing.[22] In a similar manner, modifying mixed-ligand shells to tune the hydrophobicity has been used to coordinate the formation of nanoparticle superstructures.[23] For catalysis applications, ligand exchange has been used to improve the C−C coupling rate[24] as well as H_2 production.[25] Furthermore, quantum dots (QDs) are frequently treated with additives such as HF and Zn^{2+} in order to improve photoluminescent quantum yields by removing defects such as dangling bonds at the surface.[26−28] Finally, postsynthetic ligand modification is required for tuning interparticle charge and exciton transfer in thin films of colloidal semiconductor nanocrystals.[29] The nature of these applications implicitly requires postsynthetic surface modification because the resulting surface chemistries would otherwise be significantly altered or the chemistry would preclude particle nucleation and growth.[30] Therefore, a robust understanding of the ligand behavior not only directly benefits nanoparticle synthetic design but also can enable it to be separately optimized and better compartmentalized from applications.

Previous work in the literature has elegantly defined the binding affinities and characteristics of common ligands in the cases of CdSe,[31−34] PbS,[35,36] and perovskites.[37,38] Using NMR spectroscopy, it has been shown that equilibrium models for the binding of ligands on these surfaces can be accurately and easily measured. These previous analyses, however, suffer from fundamental limitations of measuring the ensemble properties of inherently polydisperse samples. Because these systems are not perfectly uniform and vary with respect to the particle size, and, moreover, the number and type of binding sites, simplifying assumptions must be made or the model must take these factors into consideration. This greatly complicates the modeling, reducing the translatability and interpretation across particle sizes, compositions, and morphologies. Critically, many of these systems lack experimental quantification of ligand binding

Received: December 18, 2018

DOI: 10.1021/acs.inorgchem.8b03524
Inorg. Chem. XXXX, XXX, XXX−XXX

modes in the first place, relying on theory or analogy to distantly related molecular structures. Here we illustrate the veracity of using the precisely known $In_{37}P_{20}X_{51}$ (X = carboxylate) cluster as a model for the InP nanocrystal surface. This cluster can be synthesized and purified on a large scale, and its surface chemistry is precisely known from single-crystal X-ray diffraction analysis.[39] Notably, despite the rising prominence of InP nanocrystals for emissive applications, no such investigation into the ligation and surface binding properties of InP has been performed to date.

In order to answer outstanding questions surrounding InP nanoparticle surface chemistry, we adopt an analytical ^{1}H NMR spectroscopic approach used to great success in the CdSe and PbS literature.[31,35,40] Traditional aliphatic ligands are not diagnostically useful in the ^{1}H NMR spectrum of nanoparticles because of the excessive overlapping and polydispersity of their alkyl resonances in the upfield region. By using alkene-labeled ligands, it is possible to quantitatively measure both free and bound ligands on the nanoparticle surface in the relatively clean 4.0−6.0 ppm region. It is convenient for our purposes then to use oleate ligands bearing an internal alkene on the native particle surface in conjunction with exchanging ligands bearing terminal alkenes to enable a complete deconvolution and analytical assessment of the ligand-exchange equilibria. The sources of ^{1}H resonance shifts in nanoparticle solutions have recently been examined in detail, including the source of the peak shifts and broadening of ligated species.[41] By using a high-field instrument, ligated molecules can be reliably shifted and deconvoluted from their free counterparts. Herein we will use these ^{1}H NMR properties to model ligand-exchange equilibria as reversible chemical processes (Scheme 1) using quantitative

Scheme 1. Reaction Scheme Showing the Equilibrium Exchange of Oleate Ligands on InP Particles for Incoming Terminal Alkene-Labeled Ligands, Including Carboxylic Acid, Phosphonic Acid, and Thiol

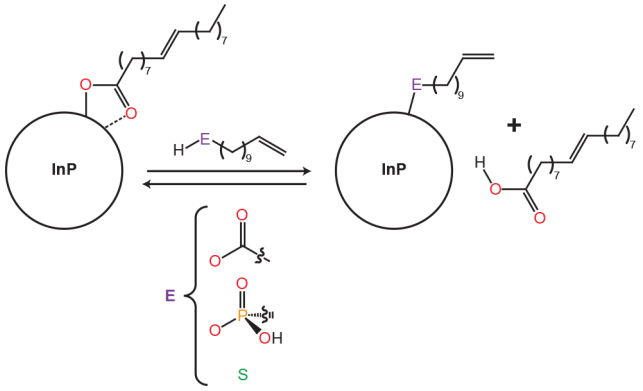

NMR integration and fitting in conjunction with mesitylene as an internal standard and a highly purified 1.3 nm $In_{37}P_{20}X_{51}$ cluster as a precise starting point. Per-particle measurements are normally highly limited by not just the polydispersity but also the inherent difficulty in determining the nanoparticle concentrations. Using an atomically defined starting point eliminates data convolution arising from ensemble measurements and allows for highly precise correlations of per-particle properties such as the ligand count and density.

RESULTS AND DISCUSSION

Carboxylate−Carboxylic Acid Exchange. Carboxylates have historically been the ligand of choice for the synthesis of InP nanoparticles both for general laboratory use and for their application in commercialized display technologies.[5] The exchange between X-type carboxylate ligands (Figure 1) such

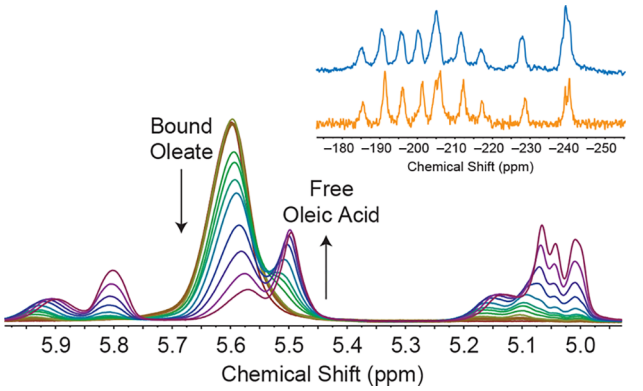

Figure 1. ^{1}H NMR spectra of the alkene region for titration of DDA into a solution of the Ol-capped $In_{37}P_{20}$ cluster, from 0 equiv (red) to 139 equiv (violet). Resonances at 5.8−5.9 and 5.0−5.2 ppm correspond to DDA, while those at 5.4−5.7 ppm correspond to Ol. Inset: ^{31}P NMR spectra of the starting cluster (blue) and the cluster + 139 equiv of DDA (orange).

as oleate (Ol) and dodec-11-enoic acid (DDA) on nanoparticle surfaces has often been modeled as a metathesis-type equilibrium, as described by eq 1.

$$[Ol]_B + [DDA]_F \underset{k_{-1}}{\overset{k_1}{\rightleftarrows}} [Ol]_F + [DDA]_B \quad (1)$$

$$K_{eq} = \frac{[Ol]_F[DDA]_B}{[Ol]_B[DDA]_F} \quad (2)$$

This model is indifferent to binding modes of the ligand and site differentiation on the nanocrystal. The crystal structure of the $In_{37}P_{20}X_{51}$ cluster with carboxylate ligands is known and exhibits exclusively bidentate and bridging−bidentate X-type binding across a relatively uniform surface. Attempting to model the exchange as an X-type metathesis and to determine K_{eq} via eq 2 shows a nonlinear trend that can be interpreted as two distinct equilibrium regimes (Figure 2A). The difference in these regimes is much greater than would be expected from the difference in the chemical potential between facets of InP;[42] moreover, a nonstoichiometric exchange ratio is seen in the early regime with substoichiometric ligand displacement. Therefore, we consider an alternative, neutral L-type binding mode in addition to the X-type exchange to account for this increase in coverage.

To model this type of binding, we adopt a modified multisite Langmuir isotherm model (eq 3) that enables us to account for multiple species as well as multiple binding modes. Additional details and derivation are available in section SI 1. Equation 3 represents the binding of a titrated acid (DDA) using a multisite-competitive Langmuir isotherm, which models the bound fraction of ligand, θ_{DDA}, as a function of the free ligand concentrations and equilibrium constants. This model allows for fitting of the fraction of sites belonging to each mode per nanoparticle, the L-type equilibria of each acid, and the relative X-type binding affinity of each carboxylate, such that KX_{DDA}/

DOI: 10.1021/acs.inorgchem.8b03524
Inorg. Chem. XXXX, XXX, XXX−XXX

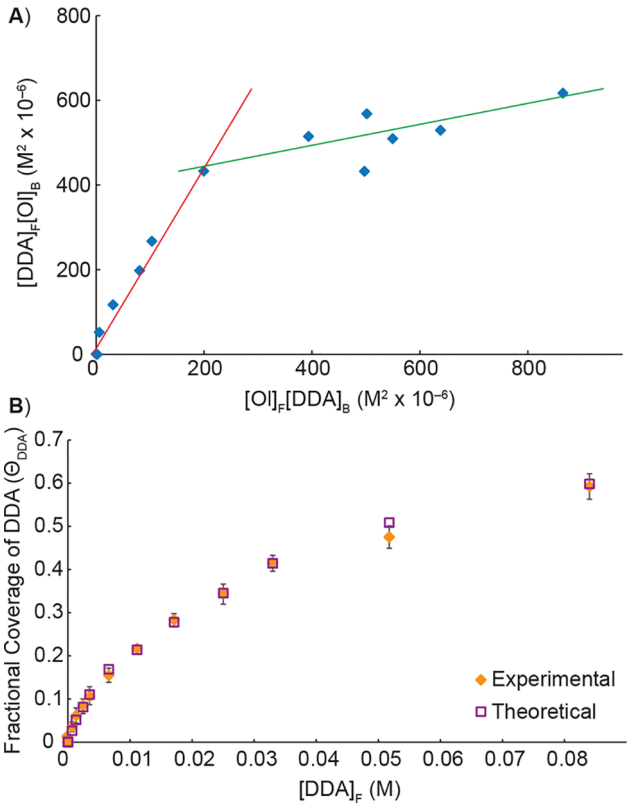

Figure 2. (A) Metathesis-style plot of K_{eq} via eq 2 for the titration of DDA into a solution of Ol-capped cluster. Instead of a single slope corresponding to K_{eq}, empirically two regimes of differing equilibrium constants are seen. (B) Same data replotted using an isotherm fit via eq 4. This fit gives the following values: KX_{eq} = 0.80, KL_{DDA} = 2.3, KL_{Ol} = 1.9, nX = 51, and nL = 8.

$KX_{Ol} = KX_{eq}$. We note that based on the range of calculated ligand desorption energies for different sites on the $In_{37}P_{20}$ cluster and the 1:1 nature of this exchange process, we would not expect to be able to distinguish individual X-type sites.[45] Considering that a ligand bound in the X- versus L-type mode will have a nearly indistinguishable terminal alkene resonance, we can further rearrange eq 3 into directly measurable concentrations for quantitative ^{1}H NMR analysis via eq 4. Using this model, we see a much-improved fit and experimentally determine the equilibrium constants (Figure 2B). Our experimental value for KX_{eq} of 0.80 is remarkably similar to that for KX_{eq} reported by Dempsey et al. for a virtually identical pair of ligands on CdSe QDs,[31] suggesting that some relative binding properties of ligands may translate very well between nanoparticle systems. This may be especially true for Cd^{2+}- and In^{3+}-based systems given the similarities in the cation size and Lewis acidity. While the basicity of carboxylic acids is well characterized[43,44] the L-type equilibria of carboxylic acids on nanoparticle surfaces have, to our knowledge, never been quantified. Here we find the equilibrium constants for the L-type binding of typical aliphatic carboxylates to be on the order of KL = 2.0 and that L-type binding accounts for approximately 15% of the total ligation when saturated. Given that L-type binding would proceed as a Lewis base interaction with a surface In ion, this ratio would likely decrease with the decreasing concentration of surface In that has been theorized and observed on larger particles.[45] Because these In sites are coordinatively saturated at the onset through bidentate binding of carboxylate, we would predict the L-type binding to be monodentate and concomitant with neighboring shifts of bound carboxylate to a monodentate binding mode in order to maintain both the coordination number and charge balance (Scheme 2).

$$\theta_{DDA} = \chi_x \frac{KX_{DDA}[DDA]_F}{1 + KX_{DDA}[DDA]_F + KX_{Ol}[Ol]_F} + \chi_l \frac{KL_{DDA}[DDA]_F}{1 + KL_{DDA}[DDA]_F + KL_{Ol}[Ol]_F} \quad (3)$$

$$[DDA]_B = [MSC]\left(nX\frac{KX_{DDA}[DDA]_F}{1 + KX_{DDA}[DDA]_F + KX_{Ol}[Ol]_F} + nL\frac{KL_{DDA}[DDA]_F}{1 + KL_{DDA}[DDA]_F + KL_{Ol}[Ol]_F}\right) \quad (4)$$

Scheme 2. Schematic Representation of L-Type Carboxylic Acid Coordination with a Concomitant Shift in a Bidentate Carboxylate to a Monodentate Binding Mode

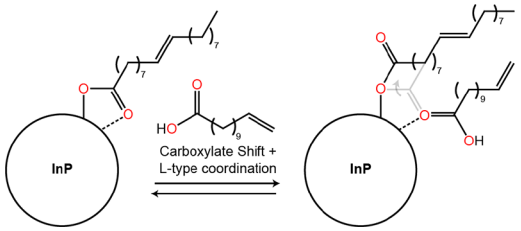

The difference between the L- and X-type binding modes was further investigated using variable-temperature ^{1}H NMR spectroscopy (Figure 3 and section SI 2). Because the

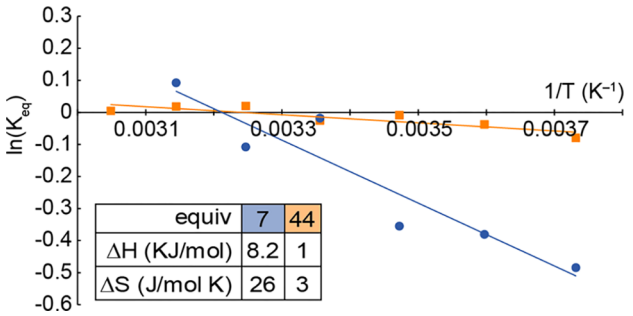

Figure 3. Van't Hoff plots for the temperature-dependent equilibria of DDA versus Ol at low-concentration (blue) versus high-concentration (orange) regimes of added DDA.

theoretical number of L-type sites is small because of steric crowding on the cluster surface and the binding is favorable, the low free acid concentration regime can be considered to be L-exchange-dominated, whereas the high free acid regime would theoretically be X-exchange-dominated and L-type-saturated. Constructing a Van't Hoff plot by examining K_{eq} as a function of the temperature in the high-concentration regime at 44 equiv of acid (115 mM acid) reveals a nearly iso-Gibbs energy reaction. This is a reasonable result given that the number of molecules in the system remains unchanged and that the acids are extremely similar to an equilibrium constant quite close to 1. By contrast, examining the low, L-type-dominated regime at 7 equiv (18 mM) reveals weakly positive enthalpy and entropy terms of ΔH° = 8 kJ/mol and ΔS° = 26 J/(mol K), respectively, in line with

DOI: 10.1021/acs.inorgchem.8b03524
Inorg. Chem. XXXX, XXX, XXX−XXX

similar measurements in the literature. These values equate to a ΔG value of 412 J/mol at room temperature and suggest that L-type binding is slightly unfavorable, whereas the isotherm fitting indicated it was slightly favorable. This may be an artifact of X-type exchange or other rearrangements convoluting the measurement; however, it would also be unsurprising that carboxylic acids bind less favorably than traditional Lewis basic L-type ligands such as amines or phosphines. Positive entropy terms for ligand-exchange reactions have been observed previously and assigned by others in the literature as disorder in the ligand shell, i.e., the entropy of mixing.[31,42] Entropy purely from mixing would, however, be proportional to the molar fractions of ligands being mixed, and thus we would expect an order of magnitude lower entropy for the low equivalent exchange regime, treated as ideal species of just 1.2 J/(mol K).[46] We have previously shown crystallographically that carboxylates have four distinct X-type binding modes on InP that are predominantly bridging and bidentate. We hypothesize that L-type carboxylate binding would be associated with local rearrangement, with neighboring ligands shifting from bidentate to monodentate in order to alleviate steric hindrance and reveal additional coordination sites. This denticity rearrangement has been seen crystallographically during the adsorption of water to the InP cluster.[47] Such a rearrangement could result in a net increase in the entropy related to the increase in available microstates of a monodentate species versus a more rigidly bound bidentate ligand. Such conformational entropies have been calculated to be on the order of 10 J/(mol K) per degree denticity in other systems.[48]

The excitonic feature of the cluster as measured by UV−vis spectroscopy was tracked as a function of the added titrant and underwent a slight 20 meV red shift followed by a 60 meV blue shift over the course of the titration at room temperature (section SI 3). This change is inconsistent with what has been seen in the Z-type etching of indium carboxylate from the cluster by amine.[47] Rather, this strongly indicates the influence of the ligand shell over the excitonic wave function, which is magnified because of the cluster's small size. Given the electronic similarity of oleic acid and DDA this shift is more attributable to changes in the surface environment as opposed to ligand identity, with changes in the binding modes and increased total coverage being the operative differences. As such, this feature is not only tunable but also highly reversible and a useful metric for conveniently tracking cluster purification. The ^{31}P NMR spectrum does not show an appreciable change upon the addition of excess carboxylic acid (Figure 1, inset). Given that exchange is fast relative to the NMR time scale and that the net density of oxygen bonds at the surface does not change, this is not surprising and supports the stability of the cluster toward excess carboxylic acid.

Carboxylate−Phosphonic Acid Exchange. Phosphonic acids are widely used in the semiconducting nanocrystal literature as robust X-type capping ligands. As ligands, they are characterized by their variable denticity binding modes and strong, often irreversible, binding affinity.[49,50] These properties have been the driving arguments for synthetic observations such as anisotropic growth[51,52] and shelling inhibition, as well as influencing the physical properties of nanoparticles through enhanced thermal, photochemical, and oxidative stability.[53−55] In the case of InP, phosphonate capping ligands have been little explored, and no bottom-up syntheses of InP using phosphonate ligands have been reported beyond a phosphonate-capped cluster species.[56] This is likely due to the extreme stability that these ligands impart upon low-molecular-weight, oligomeric, and cluster intermediates.

Dianionic binding of phosphonates and displacement of carboxylate are widely reported in the QD literature. This is readily predictable because phosphonic acids are roughly 3 orders of magnitude more acidic than analogous carboxylic acids and subsequent bidentate binding is heavily favored by the chelate effect.[57] Assuming the dianionic nature of the phosphonate ligand, the theoretical point of complete stoichiometric exchange on the starting Ol-ligated $In_{37}P_{20}X_{51}$ cluster by adding 10-eneundecylphosphonic acid (UDPA) is 25.5 equiv. Titrations toward this stoichiometric point at room temperature are associated with a steady blue shift of the excitonic feature in the UV−vis spectrum across a range of 10 meV, beyond which a decrease in the intensity and a loss of the lowest energy features and solution color are observed, suggesting cluster decomposition (section SI 4). The initial hypsochromic shift is reasonably attributable to what has been proposed in the literature as ligand effects on excitonic wave functions as a function of the headgroup electronegativity.[58−60] The highest occupied and lowest unoccupied molecular orbitals of the cluster are calculated to reside close to the surface and can be influenced by binding agents, as we have shown previously.[39] Additionally, the exchange of carboxylate for phosphonate ligands dictates a significant degree of surface rearrangement, corroborated by an increase in the cluster symmetry, as seen by ^{31}P NMR spectroscopy (section SI 5). During this room temperature ligand exchange, however, structural rearrangement is not equivalent to the alternate zincblende cluster structure observed from bottom-up synthesis at elevated temperatures. Rather, the $In_{37}P_{20}$ cluster core is evidently kinetically stable across the complete range of ligand exchange. By ^{1}H NMR spectroscopy, we measure the stoichiometry of this exchange between carboxylate and phosphonate to be 2.10 ± 0.06 carboxylates per phosphonic acid (Figure 4), in strong agreement with the initial hypothesis of bidentate, irreversible binding as the phosphonate dianion.

Beyond the stoichiometric point of complete exchange, there is no appearance of a free phosphonic acid resonance in ether the ^{1}H or ^{31}P{^{1}H} NMR spectra in these experiments. Coupled with bleaching of the UV−vis spectroscopic features, this suggests cluster decomposition in the presence of excess acid. The stoichiometric point of etching to form In_2PA_3 and PH_3 would be 55.5 equiv of added phosphonic acid; however, we do not observe a distinct crossover at this point. Etched PH_3 accounts for less than 3% of the phosphorus measured via ^{31}P NMR spectroscopy, and the continued absence of free phosphonic acid suggests that InP decomposition by phosphonic acid does not proceed through primarily PH_3 displacement. Instead, broadening of the bound phosphonate resonances and eventual solidification of the sample imply the formation of complex $InP(PO_3)(PO_3H)$ species. Despite this transformation being as completely forward driven as ligand exchange, it is only observed after ligand exchange is complete, prior to which at least 20 unique bound phosphonate resonances are observable in the ^{31}P NMR spectrum. Oligomeric phosphonate products such as this are likely what inhibits bottom-up growth of phosphonate-capped InP nanoparticles.

Carboxylate−Thiol Exchange. While not a general-use ligand choice for InP synthesis compared to carboxylates, thiols hold great interest in InP syntheses insofar as they relate to shelling strategies to access InP@ZnS and related heterostructures.[61,62] A preliminary treatment of the exchange

DOI: 10.1021/acs.inorgchem.8b03524
Inorg. Chem. XXXX, XXX, XXX−XXX

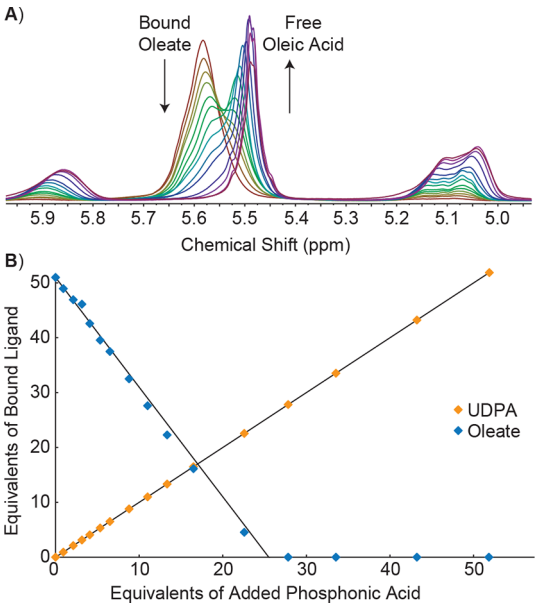

Figure 4. (A) ^{1}H NMR spectra of the alkene region for the titration of UDPA into a solution of Ol-capped $In_{37}P_{20}$ cluster, from 0 equiv (red) to 51 equiv (violet). Resonances at 5.8−5.9 and 5.0−5.2 ppm correspond to UDPA, while those at 5.4−5.7 ppm correspond to Ol. (B) Quantification of the displacement of carboxylate (blue) by phosphonic acid (orange). The solid black lines correspond to theoretical 1:1 (UDPA/UDPA, increasing) and 2:1 (DDA/UDPA, decreasing) stoichiometries, respectively.

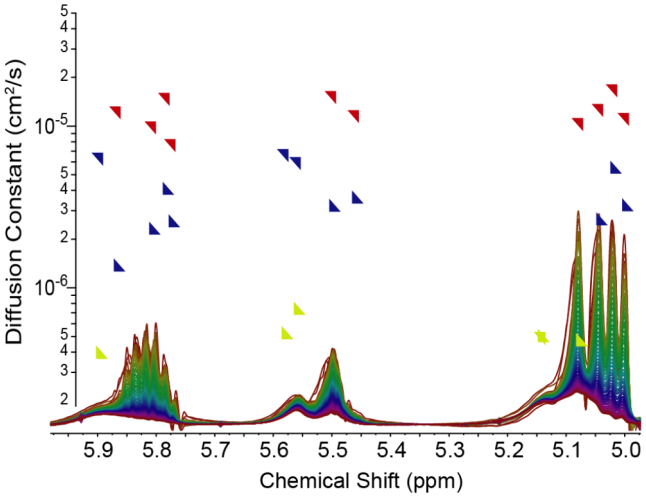

Figure 5. ^{1}H DOSY NMR spectra from low gradient (red) to high gradient (violet), overlaid with corresponding pairs of diffusion constants acquired from biexponential fitting. The mean diffusion constants in benzene and proposed assignments are as follows (cm^2/s): 1×10^{-5} (red) free acid, 5×10^{-7} (blue) etched species, and 4×10^{-6} (green) cluster.

equilibrium between 10-undecene-1-thiol (UDTh) and Ol ligands on the cluster using eq 2 results in a two-regime progression similar to that seen in the carboxylate-exchange case. Quantifying the exchange by total ligands bound per particle, however, reveals a trend inconsistent with a mixed L- and X-type binding model. The low-concentration exchange regime exhibits a highly stoichiometric 50 ± 1 total X-type-bound ligand (section SI 6). Following a rigid one-to-one exchange rate ratio strongly implies thiol does not L-type-bind to InP. Additionally, the exchange causes a significant loss of ^{31}P environment symmetry, as observed by NMR spectroscopy, which likely signifies surface reconstruction (section SI 7). This surface rearrangement appears to preclude carboxylate L-type binding, as is also observed in the case of phosphonate coordination. Modeled as pure X-type exchange, this regime follows a thiolate for carboxylate exchange with KX_{eq} = 3.9 through 36 equiv of added thiol, meaning that a favorable exchange for thiol is seen through approximately 50% starting ligand substitution. This favorable binding is consistent with thiolate being a much softer Lewis base than carboxylate and In^{3+} being a relatively soft Lewis acid. By contrast, in the high-concentration regime, a roughly linear increase in the total number of bound ligands is observed at a ratio of approximately 1 per 6 equiv of thiol added, or equivalently per increase in 0.6 mM thiol.

Because there is no observed L-type binding, superstoichiometric binding in this second regime can only be explained by particle etching, exposing more metal atoms either on the surface or in solution. Similar observations have been made in the Z-type etching of CdSe nanoparticles by concentrated primary alcohols.[63] Using ^{1}H DOSY NMR spectroscopy, we measure the signal versus gradient decay rates for the bound species to be clearly nonmonoexponential (section SI 8). Polyexponential decay curves mean that a sum of diffusing products is being measured, supporting the hypothesis of particle etching. Using biexponential fitting, three distinct species are found and can be independently correlated with the chemical shifts of bound or free regions (Figure 5). These species were found to have diffusion constants $D = 1 \times 10^{-5}$, 5×10^{-7}, and 4×10^{-6} cm^2/s, which we assign as the free acid/thiol, cluster, and etched product, respectively. Accounting for solvent viscosity differences, these values are consistent with the literature.[41,64]

The etched product appears to contain both thiolate and carboxylate. Using the Stokes−Einstein equation, this material has a hydrodynamic radius of 1.0 nm, approximately 3 times that of the free acid. Specifically assigning this species is very challenging because many small oligomers can be drawn with mixed numbers of carboxylates and thiolates, especially considering the many bridging modes of carboxylate. No such decomposition was observed by ^{1}H and ^{31}P{^{1}H} NMR spectroscopy after exposing a sample of cluster to 16 equiv of thiol for 12 h, while decomposition was effectively immediate upon exposure to an excess of 35 equiv of thiol. This observation is unlike the Z-type displacement by amines on both InP[65] and CdSe,[63] where the initial displacement is very rapid and then subsequently slows, likely speaking to a different displacement mechanism. Whereas the carboxylate- and phosphonate-exchange systems were found to be relatively analogous to those found for CdSe nanoparticles, the case for thiol differs quite dramatically. There is no evidence to suggest that thiol shows L-type behavior or that thiolate irreversibly binds on InP. Additionally, no evidence for the formation of disulfides was found in the ^{1}H NMR data, which would have a diagnostic triplet at 2.5 ppm. The etched product of high-concentration thiol exposure to the InP cluster most closely resembles Z-type exchange observed in the presence of alcohols in metal chalcogenide systems.

Carboxylate−Carboxylic Acid Exchange on QDs. The $In_{37}P_{20}X_{51}$ cluster has proven to be a robust analogue for InP QDs in many regards. It possesses an In-rich stoichiometry com-

DOI: 10.1021/acs.inorgchem.8b03524
Inorg. Chem. XXXX, XXX, XXX−XXX

parable to that established for InP QDs, and is passivated with the same commonly used ligands. Given the cluster's greater curvature and more confined electronic structure, the similarity of the ligand affinities between cluster and nanoparticle is not immediately obvious.[66] To establish the veracity of using the InP cluster as a model system for larger InP nanostructures, we have replicated the carboxylate-exchange experiment on larger InP QDs. These particles were purified in the same manner as the cluster and determined to be 3 nm by transmission electron microscopy analysis (section SI 9). Solution concentrations were determined via the literature extinction coefficient values,[66] and the exchange was carried out over a range similar to that of the cluster on a percent ligand basis using the same Ol starting and DDA titrant systems.

The results of this exchange were indeed similar to those seen in the cluster case. Attempting to model the exchange mechanism as pure X-type metathesis yielded a nonlinear fit similar to that of K_{eq} that was much-improved upon the use of isotherm fitting via eq 3 (Figure 6). The experimental value for

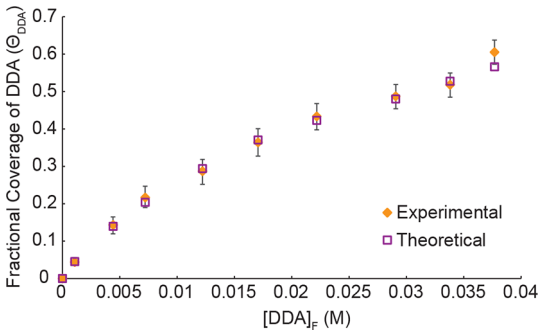

Figure 6. Isotherm fitting via eq 4 of DDA titration into a solution of Ol-capped InP QDs from 0 to 110 equiv. Fitting gives the following values: KX_{eq} = 0.88, KL_{DDA} = 2.3, KL_{Ol} = 3.5, nX = 88, and nL = 10.

the X-type equilibrium was measured to be KX_{eq} = 0.88. This value is in strong agreement with the cluster system. The ratio of L-to-X-type sites was calculated to be approximately 10% of the total sites, which is significantly less than the 15% seen in the cluster case. A decrease in the available surface-In concentration with increasing particle size has recently been computationally predicted to be as much as 30% lower for a 3.28 nm nanoparticle compared to the $In_{37}P_{20}X_{51}$ cluster.[45] This change would naturally lead to a decrease in the L-to-X-type ligand ratio because there are fewer sites in general to bind and X-type coordination takes priority for charge-balance requirements. The absolute number of bound ligands on a per-particle basis was also found to be lower than expected. At 98 bound ligands per particle, there are approximately 25% fewer bound ligands than literature and geometric considerations would otherwise predict on a per-particle basis.[45,66] This discrepancy could reasonably be attributed to ligand stripping from over-purification, as has been observed previously,[67,68] or simply an error arising from the inherent difficulty in quantifying the nanoparticle concentrations. Overall, the nanoparticle system is demonstrably similar to the cluster system with nearly equivalent relative ligand affinities in conjunction with a predictable decrease in the L-site availability.

CONCLUSIONS

Ligand shells are a complex and relatively poorly understood aspect of colloidal nanostructures. We have shown that, on colloidal InP, the ligative properties can vary greatly depending on the ligand identity but that their binding can be reliably and quantitatively modeled. By using an InP cluster as a molecularly precise starting point and alkene-labeled ligands, we are able to quantitatively model the ligand binding dynamics in an atomically precise manner using ^{1}H NMR spectroscopy. Using DDA, we demonstrate the broad similarity of the cluster coordination chemistry to that of larger QDs of InP and CdSe. By modeling the equilibrium between DDA and the starting Ol ligands using an isotherm-based approach, we are able to for the first time deconvolute and quantify carboxylic acid L-type binding to a nanoparticle surface as accounting for 10−20% of total ligand binding at saturation. Given the net increase in the entropy associated with this type of binding and the change in ^{31}P symmetry seen upon the binding of phosphonate and thiol, we suggest that both X- and L-type exchanges are concomitant with surface carboxylates shifting from bidentate to monodentate and more significant structural perturbations in the case of strongly binding ligands. UDTh was found to bind more strongly than Ol with no tendency toward L-type binding or disulfide formation, but was observed to cause decomposition prior to complete exchange. Finally, UDPA was found to bind irreversibly and at a strict 2:1 stoichiometry versus Ol, as has been observed in several material systems. This binding was largely free from decomposition below the complete exchange limit, beyond which InP phosphonate oligomers began to develop. Ultimately, we believe that observations and analytical techniques such as these will underpin future development of nanoparticle synthesis and technological translation via an improvement in the rational surface design. Methodological development in postsynthetic surface modification, including shelling for improved photophysical properties and ligand exchange for improved charge transport, will require a detailed understanding of the relative binding strengths of ligands as well as ligand decomposition pathways to achieve maximal utility.

ASSOCIATED CONTENT

Supporting Information

The Supporting Information is available free of charge on the ACS Publications website at DOI: 10.1021/acs.inorgchem.8b03524.

Full synthetic procedures and additional analytical details (PDF)

AUTHOR INFORMATION

Corresponding Author

*E-mail: cossairt@uw.edu.

ORCID

Brandi M. Cossairt: 0000-0002-9891-3259

Notes

The authors declare no competing financial interest.

ACKNOWLEDGMENTS

We gratefully acknowledge support from the University of Washington and the National Science Foundation under Grant CHE-1552164.

REFERENCES

(1) Sambur, J. B.; Chen, P. Approaches to Single-Nanoparticle Catalysis. *Annu. Rev. Phys. Chem.* **2014**, *65*, 395−422.

(2) Xia, Y.; Yang, H.; Campbell, C. T. Nanoparticles for Catalysis. *Acc. Chem. Res.* **2013**, *46*, 1671−1672.

DOI: 10.1021/acs.inorgchem.8b03524
Inorg. Chem. XXXX, XXX, XXX−XXX

(3) Semonin, O. E.; Luther, J. M.; Beard, M. C. Quantum Dots for Next-Generation Photovoltaics. *Mater. Today* **2012**, *15*, 508−515.
(4) Lewis, N. S. Toward Cost-Effective Solar Energy Use. *Science* **2007**, *315*, 798−801.
(5) Shirasaki, Y.; Supran, G. J.; Bawendi, M. G.; Bulović, V. Emergence of Colloidal Quantum-Dot Light-Emitting Technologies. *Nat. Photonics* **2013**, *7*, 13−23.
(6) Gao, X.; Yang, L.; Petros, J. A.; Marshall, F. F.; Simons, J. W.; Nie, S. In Vivo Molecular and Cellular Imaging with Quantum Dots. *Curr. Opin. Biotechnol.* **2005**, *16*, 63−72.
(7) Kairdolf, B. A.; Smith, A. M.; Stokes, T. H.; Wang, M. D.; Young, A. N.; Nie, S. Semiconductor Quantum Dots for Bioimaging and Biodiagnostic Applications. *Annu. Rev. Anal. Chem.* **2013**, *6*, 143−162.
(8) Hu, M. Z.; Zhu, T. Semiconductor Nanocrystal Quantum Dot Synthesis Approaches Towards Large-Scale Industrial Production for Energy Applications. *Nanoscale Res. Lett.* **2015**, *10*, 469.
(9) Pu, Y.; Cai, F.; Wang, D.; Wang, J.-X.; Chen, J.-F. Colloidal Synthesis of Semiconductor Quantum Dots toward Large-Scale Production: A Review. *Ind. Eng. Chem. Res.* **2018**, *57*, 1790−1802.
(10) Bukowski, T. J.; Simmons, J. H. Quantum Dot Research: Current State and Future Prospects. *Crit. Rev. Solid State Mater. Sci.* **2002**, *27*, 119−142.
(11) Johansen, J.; Stobbe, S.; Nikolaev, I. S.; Lund-Hansen, T.; Kristensen, P. T.; Hvam, J. M.; Vos, W. L.; Lodahl, P. Size Dependence of the Wavefunction of Self-Assembled InAs Quantum Dots from Time-Resolved Optical Measurements. *Phys. Rev. B: Condens. Matter Mater. Phys.* **2008**, *77*, 073303.
(12) Wang, F.; Wang, Y.; Liu, Y.-H.; Morrison, P. J.; Loomis, R. A.; Buhro, W. E. Two-Dimensional Semiconductor Nanocrystals: Properties, Templated Formation, and Magic-Size Nanocluster Intermediates. *Acc. Chem. Res.* **2015**, *48*, 13−21.
(13) Jia, G.; Xu, S.; Wang, A. Emerging Strategies for the Synthesis of Monodisperse Colloidal Semiconductor Quantum Rods. *J. Mater. Chem. C* **2015**, *3*, 8284−8293.
(14) Reiss, P.; Protière, M.; Li, L. Core/Shell Semiconductor Nanocrystals. *Small* **2009**, *5*, 154−168.
(15) Hines, D. A.; Kamat, P. V. Recent Advances in Quantum Dot Surface Chemistry. *ACS Appl. Mater. Interfaces* **2014**, *6*, 3041−3057.
(16) Owen, J. The Coordination Chemistry of Nanocrystal Surfaces. *Science* **2015**, *347*, 615−616.
(17) Talapin, D. V.; Nelson, J. H.; Shevchenko, E. V.; Aloni, S.; Sadtler, B.; Alivisatos, A. P. Seeded Growth of Highly Luminescent CdSe/CdS Nanoheterostructures with Rod and Tetrapod Morphologies. *Nano Lett.* **2007**, *7*, 2951−2959.
(18) Kim, K.; Yoo, D.; Choi, H.; Tamang, S.; Ko, J.-H.; Kim, S.; Kim, Y.-H.; Jeong, S. Halide−Amine Co-Passivated Indium Phosphide Colloidal Quantum Dots in Tetrahedral Shape. *Angew. Chem., Int. Ed.* **2016**, *55*, 3714−3718.
(19) Park, J.; Kim, S.-W. $CuInS_2$/ZnS Core/Shell Quantum Dots by Cation Exchange and Their Blue-Shifted Photoluminescence. *J. Mater. Chem.* **2011**, *21*, 3745−3750.
(20) Wang, X.-S.; Dykstra, T. E.; Salvador, M. R.; Manners, I.; Scholes, G. D.; Winnik, M. A. Surface Passivation of Luminescent Colloidal Quantum Dots with Poly(Dimethylaminoethyl Methacrylate) through a Ligand Exchange Process. *J. Am. Chem. Soc.* **2004**, *126*, 7784−7785.
(21) Groeneveld, E.; Witteman, L.; Lefferts, M.; Ke, X.; Bals, S.; Van Tendeloo, G.; de Mello Donega, C. Tailoring ZnSe−CdSe Colloidal Quantum Dots via Cation Exchange: From Core/Shell to Alloy Nanocrystals. *ACS Nano* **2013**, *7*, 7913−7930.
(22) Petryayeva, E.; Algar, W. R.; Medintz, I. L. Quantum Dots in Bioanalysis: A Review of Applications across Various Platforms for Fluorescence Spectroscopy and Imaging. *Appl. Spectrosc.* **2013**, *67*, 215−252.
(23) Merg, A. D.; Zhou, Y.; Smith, A. M.; Millstone, J. E.; Rosi, N. L. Ligand Exchange for Controlling the Surface Chemistry and Properties of Nanoparticle Superstructures. *ChemNanoMat* **2017**, *3*, 745−749.
(24) Zhang, Z.; Edme, K.; Lian, S.; Weiss, E. A. Enhancing the Rate of Quantum-Dot-Photocatalyzed Carbon−Carbon Coupling by Tuning the Composition of the Dot's Ligand Shell. *J. Am. Chem. Soc.* **2017**, *139*, 4246−4249.
(25) Chang, C. M.; Orchard, K. L.; Martindale, B. C. M.; Reisner, E. Ligand Removal from CdS Quantum Dots for Enhanced Photocatalytic H_2 Generation in PH Neutral Water. *J. Mater. Chem. A* **2016**, *4*, 2856−2862.
(26) Samadpour, M.; Boix, P. P.; Giménez, S.; Iraji Zad, A.; Taghavinia, N.; Mora-Seró, I.; Bisquert, J. Fluorine Treatment of TiO_2 for Enhancing Quantum Dot Sensitized Solar Cell Performance. *J. Phys. Chem. C* **2011**, *115*, 14400−14407.
(27) Shahid, R.; Gorlov, M.; El-Sayed, R.; Toprak, M. S.; Sugunan, A.; Kloo, L.; Muhammed, M. Microwave Assisted Synthesis of ZnS Quantum Dots Using Ionic Liquids. *Mater. Lett.* **2012**, *89*, 316−319.
(28) Stein, J. L.; Mader, E. A.; Cossairt, B. M. Luminescent InP Quantum Dots with Tunable Emission by Post-Synthetic Modification with Lewis Acids. *J. Phys. Chem. Lett.* **2016**, *7*, 1315−1320.
(29) Talapin, D. V.; Murray, C. B. PbSe Nanocrystal Solids for N- and p-Channel Thin Film Field-Effect Transistors. *Science* **2005**, *310*, 86−89.
(30) Wall, M. A.; Cossairt, B. M.; Liu, J. T. C. Reaction-Driven Nucleation Theory. *J. Phys. Chem. C* **2018**, *122*, 9671−9679.
(31) Knauf, R. R.; Lennox, J. C.; Dempsey, J. L. Quantifying Ligand Exchange Reactions at CdSe Nanocrystal Surfaces. *Chem. Mater.* **2016**, *28*, 4762−4770.
(32) Anderson, N. C.; Hendricks, M. P.; Choi, J. J.; Owen, J. S. Ligand Exchange and the Stoichiometry of Metal Chalcogenide Nanocrystals: Spectroscopic Observation of Facile Metal-Carboxylate Displacement and Binding. *J. Am. Chem. Soc.* **2013**, *135*, 18536−18548.
(33) Weiss, E. A. Organic Molecules as Tools to Control the Growth, Surface Structure, and Redox Activity of Colloidal Quantum Dots. *Acc. Chem. Res.* **2013**, *46*, 2607−2615.
(34) Zhou, Y.; Buhro, W. E. Reversible Exchange of L-Type and Bound-Ion-Pair X-Type Ligation on Cadmium Selenide Quantum Belts. *J. Am. Chem. Soc.* **2017**, *139*, 12887−12890.
(35) Kessler, M. L.; Starr, H. E.; Knauf, R. R.; Rountree, K. J.; Dempsey, J. L. Exchange Equilibria of Carboxylate-Terminated Ligands at PbS Nanocrystal Surfaces. *Phys. Chem. Chem. Phys.* **2018**, *20*, 23649−23655.
(36) Moreels, I.; Justo, Y.; De Geyter, B.; Haustraete, K.; Martins, J. C.; Hens, Z. Size-Tunable, Bright, and Stable PbS Quantum Dots: A Surface Chemistry Study. *ACS Nano* **2011**, *5*, 2004−2012.
(37) Wheeler, L. M.; Sanehira, E. M.; Marshall, A. R.; Schulz, P.; Suri, M.; Anderson, N. C.; Christians, J. A.; Nordlund, D.; Sokaras, D.; Kroll, T.; et al. Targeted Ligand-Exchange Chemistry on Cesium Lead Halide Perovskite Quantum Dots for High-Efficiency Photovoltaics. *J. Am. Chem. Soc.* **2018**, *140*, 10504−10513.
(38) Zhou, L.; Yu, K.; Yang, F.; Cong, H.; Wang, N.; Zheng, J.; Zuo, Y.; Li, C.; Cheng, B.; Wang, Q. Insight into the Effect of Ligand-Exchange on Colloidal $CsPbBr_3$ Perovskite Quantum Dot/Mesoporous-TiO_2 Composite-Based Photodetectors: Much Faster Electron Injection. *J. Mater. Chem. C* **2017**, *5* (25), 6224−6233.
(39) Gary, D. C.; Flowers, S. E.; Kaminsky, W.; Petrone, A.; Li, X.; Cossairt, B. M. Single-Crystal and Electronic Structure of a 1.3 nm Indium Phosphide Nanocluster. *J. Am. Chem. Soc.* **2016**, *138*, 1510−1513.
(40) De Nolf, K.; Cosseddu, S. M.; Jasieniak, J. J.; Drijvers, E.; Martins, J. C.; Infante, I.; Hens, Z. Binding and Packing in Two-Component Colloidal Quantum Dot Ligand Shells: Linear versus Branched Carboxylates. *J. Am. Chem. Soc.* **2017**, *139*, 3456−3464.
(41) De Roo, J.; Yazdani, N.; Drijvers, E.; Lauria, A.; Maes, J.; Owen, J. S.; Van Driessche, I.; Niederberger, M.; Wood, V.; Martins, J. C.; et al. Probing Solvent−Ligand Interactions in Colloidal Nanocrystals by the NMR Line Broadening. *Chem. Mater.* **2018**, *30*, 5485−5492.
(42) Cho, E.; Jang, H.; Lee, J.; Jang, E. Modeling on the Size Dependent Properties of InP Quantum Dots: A Hybrid Functional Study. *Nanotechnology* **2013**, *24*, 215201.
(43) Lee, D. G.; Sadar, M. H. The Basicity of Aliphatic Carboxylic Acids. *Can. J. Chem.* **1976**, *54*, 3464−3469.

DOI: 10.1021/acs.inorgchem.8b03524
Inorg. Chem. XXXX, XXX, XXX−XXX

(44) Böhm, S.; Exner, O. Basicity of Carboxylic Acids: Resonance in the Cation and Substituent Effects. *New J. Chem.* **2005**, *29*, 336−342.
(45) Zhao, Q.; Kulik, H. J. Electronic Structure Origins of Surface-Dependent Growth in III−V Quantum Dots. *Chem. Mater.* **2018**, *30*, 7154−7165.
(46) Denbigh, K. *The Principles of Chemical Equilibrium*, 3rd ed.; Cambridge University Press, 1971.
(47) Gary, D. C.; Petrone, A.; Li, X.; Cossairt, B. M. Investigating the Role of Amine in InP Nanocrystal Synthesis: Destabilizing Cluster Intermediates by Z-Type Ligand Displacement. *Chem. Commun.* **2017**, *53*, 161−164.
(48) Gaberle, J.; Gao, D. Z.; Watkins, M. B.; Shluger, A. L. Calculating the Entropy Loss on Adsorption of Organic Molecules at Insulating Surfaces. *J. Phys. Chem. C* **2016**, *120*, 3913−3921.
(49) Wagner, G. W.; Fry, R. A. Observation of Distinct Surface Al $_{IV}$ Sites and Phosphonate Binding Modes in γ-Alumina and Concrete by High-Field ^{27}Al and ^{31}P MAS NMR. *J. Phys. Chem. C* **2009**, *113*, 13352−13357.
(50) Owen, J. S.; Park, J.; Trudeau, P.-E.; Alivisatos, A. P. Reaction Chemistry and Ligand Exchange at Cadmium−Selenide Nanocrystal Surfaces. *J. Am. Chem. Soc.* **2008**, *130*, 12279−12281.
(51) Peng, Z. A.; Peng, X. Mechanisms of the Shape Evolution of CdSe Nanocrystals. *J. Am. Chem. Soc.* **2001**, *123*, 1389−1395.
(52) Wang, F.; Tang, R.; Kao, J. L.-F.; Dingman, S. D.; Buhro, W. E. Spectroscopic Identification of Tri- *n* -Octylphosphine Oxide (TOPO) Impurities and Elucidation of Their Roles in Cadmium Selenide Quantum-Wire Growth. *J. Am. Chem. Soc.* **2009**, *131*, 4983−4994.
(53) Prodanov, M. F.; Pogorelova, N. V.; Kryshtal, A. P.; Klymchenko, A. S.; Mely, Y.; Semynozhenko, V. P.; Krivoshey, A. I.; Reznikov, Y. A.; Yarmolenko, S. N.; Goodby, J. W.; Vashchenko, V. V. Thermodynamically Stable Dispersions of Quantum Dots in a Nematic Liquid Crystal. *Langmuir* **2013**, *29*, 9301−9309.
(54) Tang, J.; Brzozowski, L.; Barkhouse, D. A. R.; Wang, X.; Debnath, R.; Wolowiec, R.; Palmiano, E.; Levina, L.; Pattantyus-Abraham, A. G.; Jamakosmanovic, D.; Sargent, E. H. Quantum Dot Photovoltaics in the Extreme Quantum Confinement Regime: The Surface-Chemical Origins of Exceptional Air- and Light-Stability. *ACS Nano* **2010**, *4*, 869−878.
(55) Xuan, T.; Yang, X.; Lou, S.; Huang, J.; Liu, Y.; Yu, J.; Li, H.; Wong, K.-L.; Wang, C.; Wang, J. Highly Stable CsPbBr3 Quantum Dots Coated with Alkyl Phosphate for White Light-Emitting Diodes. *Nanoscale* **2017**, *9*, 15286−15290.
(56) Gary, D. C.; Terban, M. W.; Billinge, S. J. L.; Cossairt, B. M. Two-Step Nucleation and Growth of InP Quantum Dots via Magic-Sized Cluster Intermediates. *Chem. Mater.* **2015**, *27*, 1432−1441.
(57) Franz, R. G. Comparisons of PKa and Log P Values of Some Carboxylic and Phosphonic Acids: Synthesis and Measurement. *AAPS PharmSci* **2001**, *3*, 1−13.
(58) Kroupa, D. M.; Vörös, M.; Brawand, N. P.; McNichols, B. W.; Miller, E. M.; Gu, J.; Nozik, A. J.; Sellinger, A.; Galli, G.; Beard, M. C. Tuning Colloidal Quantum Dot Band Edge Positions through Solution-Phase Surface Chemistry Modification. *Nat. Commun.* **2017**, *8*, 15257.
(59) Frederick, M. T.; Weiss, E. A. Relaxation of Exciton Confinement in CdSe Quantum Dots by Modification with a Conjugated Dithiocarbamate Ligand. *ACS Nano* **2010**, *4*, 3195−3200.
(60) Giansante, C. Surface Chemistry Control of Colloidal Quantum Dot Band Gap. *J. Phys. Chem. C* **2018**, *122*, 18110−18116.
(61) Bang, E.; Choi, Y.; Cho, J.; Suh, Y.-H.; Ban, H. W.; Son, J. S.; Park, J. Large-Scale Synthesis of Highly Luminescent InP@ZnS Quantum Dots Using Elemental Phosphorus Precursor. *Chem. Mater.* **2017**, *29*, 4236−4243.
(62) Ryu, E.; Kim, S.; Jang, E.; Jun, S.; Jang, H.; Kim, B.; Kim, S.-W. Step-Wise Synthesis of InP/ZnS Core−Shell Quantum Dots and the Role of Zinc Acetate. *Chem. Mater.* **2009**, *21*, 573−575.
(63) Anderson, N. C.; Hendricks, M. P.; Choi, J. J.; Owen, J. S. Ligand Exchange and the Stoichiometry of Metal Chalcogenide Nanocrystals: Spectroscopic Observation of Facile Metal-Carboxylate Displacement and Binding. *J. Am. Chem. Soc.* **2013**, *135*, 18536−18548.
(64) White, J. R. Diffusion Coefficients of Fatty Acids and Monobasic Phosphoric Acids in *n* -Decane. *J. Chem. Phys.* **1955**, *23*, 2247−2251.
(65) Gary, D. C.; Petrone, A.; Li, X.; Cossairt, B. M. Investigating the Role of Amine in InP Nanocrystal Synthesis: Destabilizing Cluster Intermediates by Z-Type Ligand Displacement. *Chem. Commun.* **2017**, *53*, 161−164.
(66) Xie, L.; Shen, Y.; Franke, D.; Sebastián, V.; Bawendi, M. G.; Jensen, K. F. Characterization of Indium Phosphide Quantum Dot Growth Intermediates Using MALDI-TOF Mass Spectrometry. *J. Am. Chem. Soc.* **2016**, *138*, 13469−13472.
(67) Roberge, A.; Stein, J. L.; Shen, Y.; Cossairt, B. M.; Greytak, A. B. Purification and In Situ Ligand Exchange of Metal-Carboxylate-Treated Fluorescent InP Quantum Dots via Gel Permeation Chromatography. *J. Phys. Chem. Lett.* **2017**, *8*, 4055−4060.
(68) Doris, S. E.; Lynch, J. J.; Li, C.; Wills, A. W.; Urban, J. J.; Helms, B. A. Mechanistic Insight into the Formation of Cationic Naked Nanocrystals Generated under Equilibrium Control. *J. Am. Chem. Soc.* **2014**, *136*, 15702−15710.

DOI: 10.1021/acs.inorgchem.8b03524
Inorg. Chem. XXXX, XXX, XXX−XXX